Magnetic-Responsive Hybrids of Fe_3O_4 Nanoparticles with β-Lactoglobulin Amyloid Fibrils and Nanoclusters

Sreenath Bolisetty, Jijo J. Vallooran, Jozef Adamcik, and Raffaele Mezzenga*

Department of Health Science and Technology, Food and Soft Materials Laboratory, ETH Zurich, Schmelzbergstrasse 9, LFO-E22, CH-8092 Zurich, Switzerland

ABSTRACT We report on the synthesis and magnetic-responsive behavior of hybrids formed by dispersing negatively charged iron oxide (Fe_3O_4) magnetic nanoparticles in positively charged β-lactoglobulin protein solutions at acidic pH, followed by heating at high temperatures. Depending on the pH used, different hybrid aggregates can be obtained, such as nanoparticle-modified amyloid fibrils (pH 3) and spherical nanoclusters (pH 4.5). We investigate the effect of magnetic fields of varying strengths (0−5 T) on the alignment of these Fe_3O_4-modified amyloid fibrils and spherical nanoclusters using a combination of scattering, birefringence and microscopic techniques and we find a strong alignment of the hybrids upon increasing the intensity of the magnetic field, which we quantify *via* 2D and 3D order parameters. We also demonstrate the possibility of controlling magnetically the sol−gel behavior of these hybrids: addition of salt (NaCl, 150 mM) to a solution containing nanoparticles modified with β-lactoglobulin amyloid fibrils (2 wt % fibrils modified with 0.6 wt % Fe_3O_4 nanoparticles) induces first the formation of a reversible gel, which can then be converted back to solution upon application of a moderate magnetic field of 1.1 T. These hybrids offer a new appealing functional colloidal system in which the aggregation, orientational order and rheological behavior can be efficiently controlled in a purely noninvasive way by external magnetic fields of weak intensity.

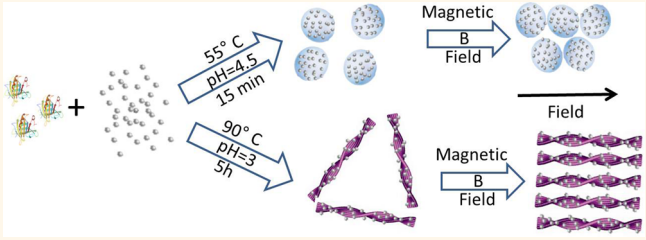

KEYWORDS: β-lactoglobulin amyloid fibrils · microgels · nanoclusters · hybrid iron-oxide protein aggregates · alignment · stimuli responsive · sol−gel transition

Development of bioinorganic hybrid nanomaterials[1] with advanced properties and improved performance[2] is receiving considerable interest due to the possibility to achieve biocompatibility[3,4] and to trigger novel nanotechnological applications.[5,6] Special interest has been devoted to biotemplated magnetic nanomaterials[7,8] due to their potential use[9] in medical diagnostics[10,11] as contrast agents,[12] biosensing agents[13] and therapeutic agents,[14] but also due to their relevance in high-density data storage units.[15] In particular, magnetic hybrids offer the possibility to achieve high spatial order and alignment,[16] which is a highly desirable feature in several applications.[17,18] For example, aligned ZnO nanowire arrays[19] and liquid crystalline arranged CdSe[20] nanorods can produce stable and continuous direct current output, whereas aligned carbon nanotubes have been shown to improve the overall mechanical properties of hybrid materials.[21]

Several techniques and strategies[22] have been considered to achieve high spatial alignment of hybrid nanostructures,[23,24] such as physical and chemical vapor deposition techniques,[25] biorecognition,[26] orientation growth on substrates,[27] exploitation of liquid crystalline or fluidic interactions, Langmuir−Blodgett[28] transfer and exposure to external electric[29] and magnetic fields.[30,31] Within all these techniques, the alignment induced by an external applied magnetic field is highly preferable in several aspects, as this can be, at the same time, noninvasive in nature, of low cost, and relatively easy to be implemented. However, due to the low magnetic susceptibility of organic matter,[32] inorganic magnetic nanoparticles[33] often have to be attached to the starting constituents in order to generate improved response to magnetic fields.[34−36]

External magnetic fields can also be used in combination with other techniques to produce three-dimensional alignment of bioinspired nanohybrids. For example, Reches *et al.* demonstrated that external magnetic fields can control the horizontal alignment of aromatic peptide nanotubes noncovalently

* Address correspondence to raffaele.mezzenga@hest.ethz.ch.

Received for review April 21, 2013 and accepted June 10, 2013.

Published online June 10, 2013
10.1021/nn401988m

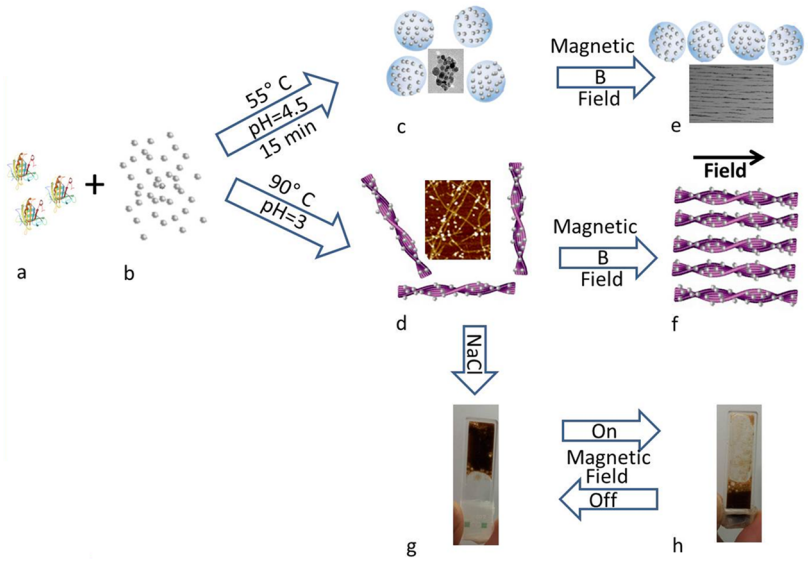

Figure 1. Schematic illustration of the preparation of magnetic-responsive amyloid fibrils and spherical nanoclusters, and their alignment in presence of a magnetic field. (a) β-Lactoglobulin protein monomers. (b) Magnetic Fe_3O_4 nanoparticles. (c) Formation of nanoparticle-modified spherical nanoclusters at pH 4.5; corresponding TEM image. (d) Self-assembly of the protein monomers and Fe_3O_4 nanoparticles into nanoparticle-modified amyloid fibrils; corresponding AFM image. Alignment of (e) nanoparticle modified spherical nanoclusters and (f) the amyloid fibrils after application of the magnetic field (B). (g) Gel formation after addition of NaCl to the nanoparticle modified amyloid fibrils and their (h) reversible solution transition with application of magnetic field.

bonded to ferrofluids and vertical aligned peptide nanoforest growth achieved by chemical vapor deposition method.[25]

β-Lactoglobulin contains a diverse complement of amino acids, making it a versatile protein for the directed synthesis of hybrid gold,[37] titanium dioxide[38] and magnetic inorganic structures.[39] Here, we discuss the synthesis of a new type of bioinspired hybrids, consisting of Fe_3O_4 magnetic nanoparticles and β-lactoglobulin protein aggregates, the latter in the form of either amyloid fibrils or spherical nanoclusters. Mixing the negatively charged magnetic nanoparticles and positively charged protein solution causes the electrostatic complexation of nanoparticles and proteins, which after heating of the solution at acidic pH undergo unfolding and aggregation. The pH of the solution settles the final structure of the self-assembled bioinorganic hybrid aggregates. Fe_3O_4 magnetic nanoparticle-modified amyloid fibrils are formed at pH 3, whereas Fe_3O_4 magnetic nanoparticle-modified spherical nanoclusters are obtained at pH 4.5. We then show that these self-assembled magnetic biohybrids can be aligned in three dimensions by magnetic fields as low as 0.1 T. We study in detail the orientational order of these hybrids at increasing magnetic fields by small angle neutron scattering (SANS), birefringence, optical and atomic force microscopy (AFM) techniques. We also show the possibility of magnetically and reversibly controlling the sol–gel behavior[40,41] of these hybrids: with the addition of 150 mM NaCl salt to the Fe_3O_4-nanoparticle modified amyloid fibrils, the system undergoes a sol–gel transition due to the screened electrostatic repulsion among fibrils and the dominating behavior of hydrophobic attractions.[42] However, upon application of 1.1 T to the gel, the amyloid fibrils align, inducing a backward gel–sol transition, which can again be suppressed when the magnetic field is released. Thus, the present system offers a new type of bioinspired hybrids in which the collective colloidal behavior and corresponding rheological properties can be controlled reversibly and noninvasively by an external magnetic field.

RESULTS AND DISCUSSION

Figure 1 summarizes the preparation of the nanoparticle-modified spherical nanoclusters, and amyloid fibrils together with their alignment and gel-to-solution transition in presence of a magnetic field. Initially, mixing β-lactoglobulin protein monomers (Figure 1a) with magnetic nanoparticles (Figure 1b) causes the formation of electrostatic complexes. A combination of heat treatment and acidic pH induces protein denaturation and aggregate formation. The structure of the aggregates could be fine-tuned by varying pH and temperature. At pH 4.5, magnetic nanoparticles modified spherical nanoclusters formed after 15 min of heat treatment at 55 °C (see Figure 1c for a schematic and corresponding TEM image). At pH 3, magnetic nanoparticles modified amyloid structures formed after 5 h of heat treatment at 90 °C (see Figure 1d for a schematic and corresponding AFM image). The ratio of protein/nanoparticles in both the fibrils and the spherical aggregates can be altered by varying the initial weight fractions of the two components. As it will be shown later in this manuscript, both hybrid structures have ability to align in the direction of magnetic field (Figure 1e,f). Below, we discuss the main results by the

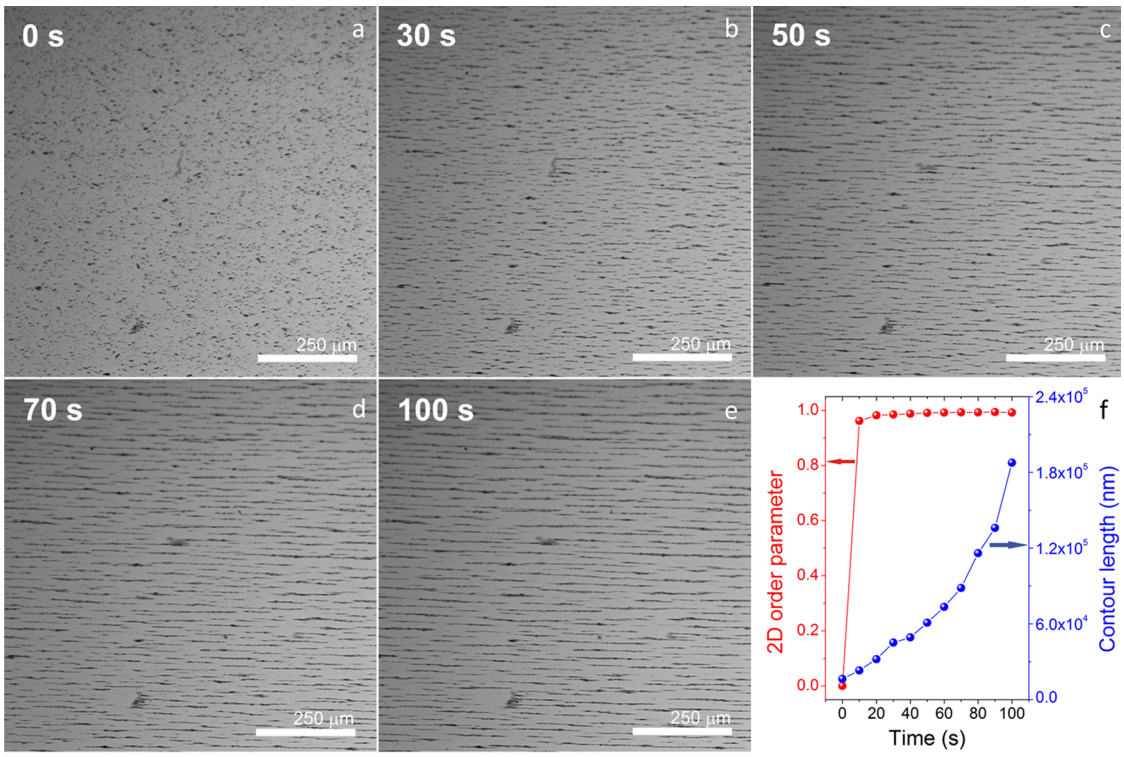

Figure 2. Optical microscopy images of the nanoparticle-modified β-lactoglobulin spherical nanoclusters formed at 2 wt % protein concentration and pH 4.5 and their alignment after application of a horizontal 0.1 T magnetic field after a time of (a) 0 s, (b) 30 s, (c) 50 s, (d) 70 s, (e) 100 s. (f) Variation of the 2D order parameter and average contour length of clusters *versus* time of exposure to the external magnetic field.

class of hybrid aggregates. Additionally, the magnetic nanoparticle-modified amyloid fibrils undergo reversible gel (Figure 1g, addition of NaCl) to solution transition (Figure 1h) after application of a magnetic field.

Nanoparticle-Modified Spherical Nanoclusters. Hybrid nanoparticle clusters can be synthesized following a multitude of techniques.[43−45] In this section, we describe the process leading to protein-templated Fe_3O_4-β-lactoglobulin nanoclusters and their magnetic-responsive properties. In a typical composition, the hybrid Fe_3O_4 nanoparticle-modified spherical nanoclusters were synthesized by incubating 0.6 wt % of the 10 nm size anionic Fe_3O_4 nanoparticles (see Figure S1 of the Supporting Information) with 2 wt % of the β-lactoglobulin protein monomers at pH 4.5. The protein β-lactoglobulin undergoes microgel-like aggregation near the isoelectric point (pH 5.1),[42] leading, when heated at pH 4.5 and 55 °C for 15 min, to the final nanoparticle mediated spherical hybrid nanoclusters schematized in Figure 1 and shown in Figure 2a. The size of the cluster depends on the protein concentration as well as the nanoparticles concentration: at the β-lactoglobulin concentration of 2 wt %, the hybrid cluster is above 1 μm in size. These protein-based ferrofluids are very stable for several weeks and no precipitation, nor aggregation, is observed under rest conditions.

Figure 2b−e shows the colloidal behavior of the spherical hybrid nanoclusters in presence of an external magnetic field as observed by optical microscopy. Figure 2b clearly shows that the horizontal application of the external magnetic field of 0.1 T already after 30 s causes the self-assembling of nanoclusters to longer chain-like clusters, perfectly aligned in the field direction. A video in the Supporting Information shows the real-time growth and alignment of the magnetic nanoclusters in presence of the magnetic field. The snapshots of the video at the various times of 0, 30, 50, 70, and 100 s are shown in Figure 2, panels a, b, c, d, and e, respectively. Within a very short time, a perfect alignment is reached and the only notable effect with time is that the length of the clusters keeps increasing steadily from the micrometers to the millimeter range. The 2D order parameter of the cluster strings is calculated from the optical images using the equation $S_{2D}=\langle 2\cos^2\Theta - 1\rangle$, where Θ is the angle between any specific aggregate string and the mean orientation director η and the bracket denotes an average over all observations. The 2D order orientation parameter reaches the extremely high value of 0.99 within a few decades of seconds, indicating a nearly perfect orientational order. Interestingly, the removal of the magnetic field causes the destruction of the alignment and redispersion of the initial individual nanoclusters into a random colloidal dispersion, indicating complete reversibility of the process (see Supporting Information Figure S2).

The alignment of the spherical nanoclusters is possible in all the three-dimensional magnetic field directions as shown in Figure 3. While Figures 3a and 3b

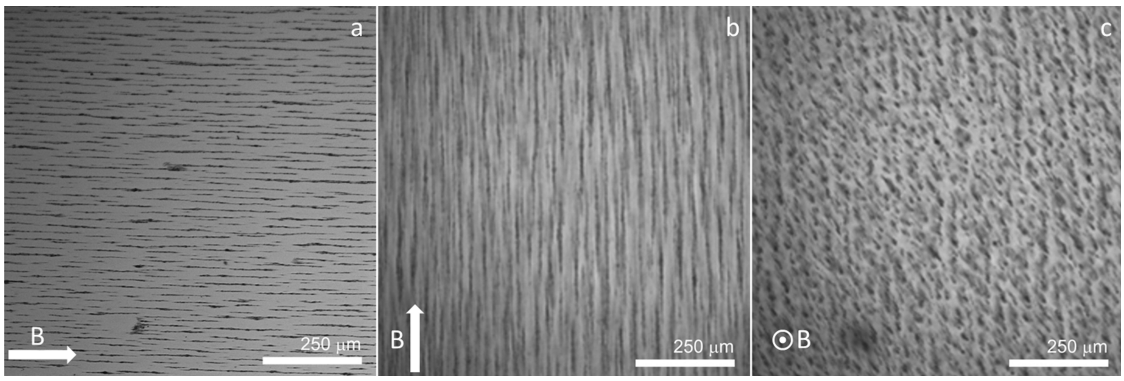

Figure 3. Optical microscopy images showing the alignment of the β-lactoglobulin Fe_3O_4 nanoparticle modified hybrid spherical nanoclusters by applying a magnetic field of 0.1 T in (a) horizontal direction, (b) vertical direction and (c) perpendicularly to the substrate plane.

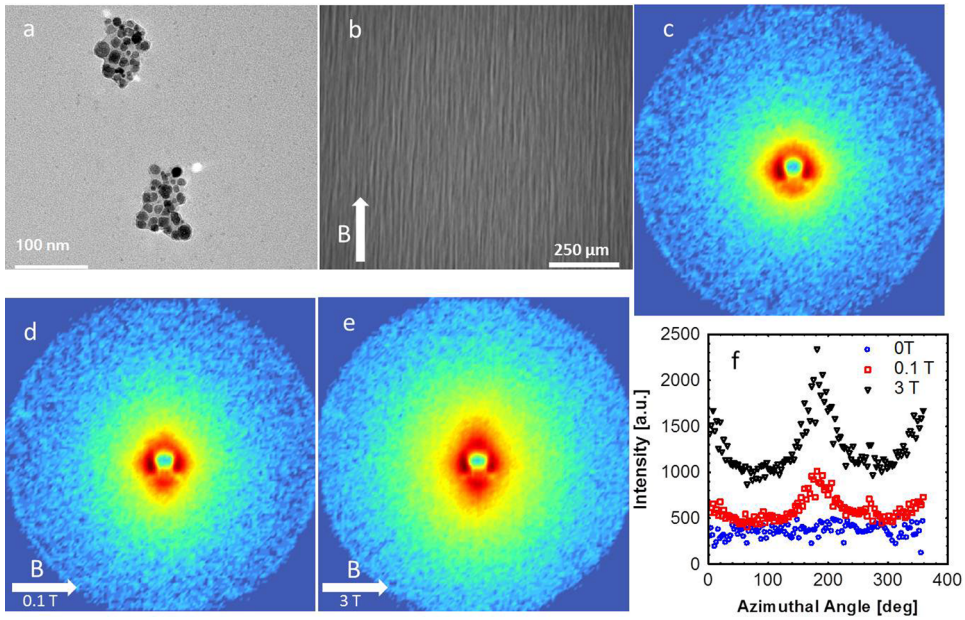

Figure 4. (a) TEM image of the nanoparticle modified spherical nanoclusters formed using 0.2 wt % of β-lactoglobulin and pH 4.5. (b) Optical microscope image of the alignment of the hybrid spherical nanoclusters along the vertically applied magnetic field. (c) SANS of the nanoparticle modified spherical nanoclusters without magnetic field. (d) SANS in presence of 0.1 T magnetic field. (e) SANS in presence of 3 T magnetic field. (f) SANS intensities as a function of the azimuthal angle at 0, 0.1, and 3 T magnetic fields, respectively.

show the alignment produced applying a magnetic field of 0.1 T in the horizontal and vertical direction, respectively, these nanoclusters can also align perpendicular to the plane of the substrate, as shown in Figure 3c, when the magnetic field is applied along this direction. In Figure 3c, a slight tilt from 90° is applied for visualization purposes. The corresponding image for a perfectly aligned magnetic field at 90° is given in the Supporting Information as Figure S3, where only point-like clusters are visible. Figure S4 of the Supporting Information shows the alignment of β-lactoglobulin spherical nanoclusters formed at the slightly different concentration of 1 wt % protein exposed at a magnetic field strength of 0.1 T.

Figure 4 shows the case of spherical hybrid nanoclusters obtained at the much lower protein concentration of 0.2 wt % and their alignment after application of magnetic fields of different strengths. The hybrid structure is first analyzed using TEM: in Figure 4a, it can clearly be observed that the Fe_3O_4 nanoparticles are self-assembled within the protein nanoclusters, the latter being polydisperse in size with an average diameter of 100 nm. Additional TEM images are shown in Supporting Information (Figure S5). Thus, the size obtained for the nanoparticle-modified spherical nanoclusters at 0.2 wt % β-lactoglobulin protein concentration is much smaller compared to the corresponding hybrids prepared at 2 wt % protein, illustrating how the aggregate structure and size depend directly on the initial protein concentration. The optical microscopy image in Figure 4b shows that these smaller nanoclusters still align efficiently upon application of the magnetic field of intensity 0.1 T, following a mechanism analogous to what is observed for the

larger spherical nanoclusters (Figure 3). Similar to the larger homologues, these structures relax to the isotropic fluid after removing the magnetic field. We then studied the effect of magnetic field intensity on the alignment of the magnetic nanoparticle modified spherical nanoclusters structures at much smaller length scales and in 3D using SANS. For the SANS measurements, the field was applied only in the horizontal direction. The orientations of the structures were investigated at the different magnetic field intensities of 0.1 and 3 T. SANS is advantageous to investigate Fe_3O_4-nanoparticles mediated alignment because the scattering length of the Fe_3O_4 nanoparticles is similar to that of the background solvent D_2O,[46] so that a contrast matching is realized and we obtain the main scattering intensity primarily from the protein aggregate structures.

The SANS intensity is isotropic without applying the magnetic field, as shown in Figure 4c, where the corresponding 2D SANS profile is given. The corresponding scattering intensity, averaged radially between scattering vectors of 0.07 and 0.25 nm^{-1} and plotted as a function of the azimuthal angle, confirms isotropic alignment of the aggregates, as shown in Figure 4f. The SANS measurement of the same sample is then measured after applying 0.1 T magnetic field, as shown in Figure 4d. The scattering intensity changes from isotropic to anisotropic in presence of the magnetic field, as revealed by the anisotropic scattering profile, where two polar maxima indicate orientation of the clusters in the horizontal axis, *i.e.*, parallel to the applied magnetic field. The magnetic field strength is then further increased to 3 T and the corresponding SANS 2D diffractogram is shown in Figure 4e, whereas the radially averaged scattering intensity *versus* azimuthal angle is given at the different magnetic field strengths in Figure 4f. Therefore, it can clearly be concluded that an increase in intensity of the magnetic field induces the distribution of the scattered intensity to becomes progressively more peaked, witnessing an increased orientation in the magnetic field direction. The radially averaged intensities and the quality of the alignment were further quantified by extracting the 3D orientation order parameter by:[47]

$$S_{3D} = \frac{\int_0^{\pi/2} I(\Theta)(3\cos^2\Theta - 1)\sin\Theta\partial\Theta}{\int_0^{\pi/2} I(\Theta)\sin\Theta\partial\Theta} \quad (1)$$

The 3D orientation order parameter quantified in eq 1 is found to have a value of 0.42 at the magnetic field of 0.1T; however, the order parameter increases to 0.68 when the magnetic field intensity is increased to 3 T, confirming, quantitatively that the level of order can be controlled directly by the intensity of the applied magnetic field.

Nanoparticle-Modified Amyloid Fibrils. We then investigated the effect of exposure to an external magnetic field on the nanoparticle-modified amyloid fibrils.

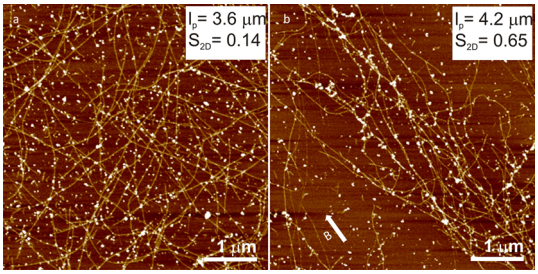

Figure 5. AFM images of iron nanoparticles modified amyloid fibrils: (a) without applying the magnetic field and (b) after applying the external magnetic field of 1.1 T for 120 s.

Protein fibrils are well-known to undergo, with increasing concentration, a first order thermodynamic transition from an isotropic to a nematic phase. This transition is purely ruled by excluded volume interactions; at higher concentrations, a sol−gel transition is observed. Our previous reports have investigated in detail these transitions at different fibril contour lengths, pH and ionic strengths.[42,48] Here we are primarily centering the study on the role that the magnetic field plays on their alignment; for this reason, we chose to work, in most of the results presented below, just underneath the isotropic−nematic transition, which in these thick fibril is expected at protein fibrils concentration above 0.3 wt %.[42]

The nanoparticle-modified amyloid fibrils were prepared in a similar procedure as that followed for the spherical nanoclusters, by mixing β-lactoglobulin and magnetic nanoparticles prior to heating. However, in this case, the solution is maintained at pH 3 and heated at 90 °C for 5 h. The low acidic pH conditions used in this case induce β-lactoglobulin protein fibrils formation. The detailed structural analysis of these amyloid fibrils is given in our previous publications.[49] To start, we used (AFM) to detect and quantify the effect of the magnetic field on these hybrid fibrils. The nanoparticle modified amyloid fibrils prepared at 2 wt % were diluted to 0.1 wt % and imaged before and after exposure to an external magnetic field. A typical AFM image of the hybrid protein fibrils before exposure to a magnetic field is shown in Figure 5a. The linear amyloid fibrils decorated with nanoparticles are clearly visible. Interestingly, the conditions used in this study (*e.g.*, pH 3, *etc.*) produced fibrils with the main population peaked around a maximum height of about 6 nm, higher compared to our previous work where the main population of fibrils obtained at pH 2 had a maximum height of about 4 nm.[49] Therefore, the fibrils are more rigid with a higher persistence length of l_p = 3.6 μm; this persistence length is in good agreement with the persistence length previously found for the population with maximum height 6 nm.[49] Without exposure to a magnetic field, the fibrils were randomly oriented on the mica substrate: the 2D order parameter calculated for semiflexible objects in two dimensions is very small (S_{2D} = 0.14). Figure 5b shows the AFM image after

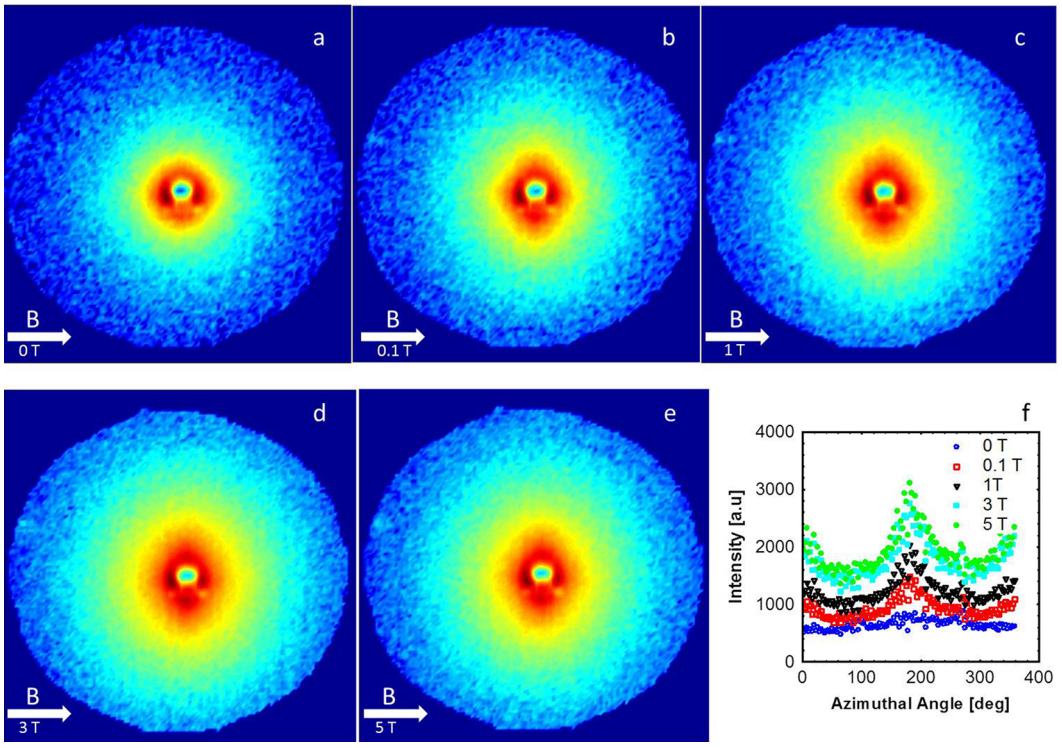

Figure 6. SANS 2D profiles for nanoparticle-modified amyloid fibrils diluted at 0.3 wt % total weight concentration and at increasing magnetic field intensities. (a) No magnetic field (0 T), (b) 0.1 T, (c) 1 T, (d) 3 T, (e) 5 T. (f) SANS intensity as a function of the azimuthal angle at the various magnetic fields considered.

applying a magnetic field of 1.1 T. The magnetic field was applied during incubation of a solution of mature hybrid fibrils on the mica substrate, during 120 s. In this case, the micrograph shows that the fibrils are prevalently aligned in the direction of the magnetic field direction, with a 2D order parameter $S_{2D} = 0.65$. Interestingly, the other visible effect produced by the presence of the magnetic field is the stretching of the fibrils in the direction of the field, with a persistence length increased to 4.2 μm. Additional AFM images before and after exposure to the magnetic field are provided in the Supporting Information (Figure S6).

The effect of the different magnetic field strengths on the alignment of the nanoparticle-modified amyloid fibrils was analyzed *via* SANS experiments, starting with a colloidal suspension prepared using 2 wt % protein and diluted to 0.3 wt % total mass. Figure 6a to Figure 6e show the SANS 2D scattering profiles at different magnetic field strengths of 0, 0.1, 1, 3, and 5 T, respectively. The corresponding azimuthal anisotropic scattering intensities are given for all cases in Figure 6f. The anisotropic scattered intensity increases in the direction perpendicular to the magnetic field direction with increasing magnetic field strength. The 3D order parameter calculated by eq 1 indicates that the order parameter of the nanoparticle-modified amyloid fibril increases from 0 to 0.38, 0.4, 0.49, and 0.52 when increasing the magnetic field strength from 0 to 0.1, 1, 3, and 5 T, respectively.

Having assessed the effect of the intensity of the magnetic field on the alignment, we then investigated the reversibility of the alignment process, that is, whether the spatial alignment is completely erasable upon removal of the magnetic field. Figure S7 of the Supporting Information shows the 2D SANS scattering profile generated by the nanoparticle-modified amyloid fibrils at three different stages before exposure, during exposure and after removing the magnetic field. The alignment of the nanoparticle-modified amyloid fibrils is demonstrated to be reversible upon exposure/removal of the magnetic field.

We also prepared hybrid magnetic protein fibrils containing three different quantities of magnetic nanoparticles on their surface by varying the initial nanoparticles concentration. The alignment of these fibrils was investigated at a constant magnetic field strength of 3 T. Figures S8a, S8b, and S8c of the Supporting Information show SANS 2D profiles of the hybrid protein fibrils prepared at an initial 2 wt % protein concentration with 0.12, 0.6, and 1.12 wt % magnetic nanoparticles, respectively, then diluted to a final 0.3 wt % total mass concentration prior to measurements. The anisotropic scattering pattern becomes sharper with increasing concentration of magnetic nanoparticles. As expected, the 3D order parameter increases from 0.43, to 0.49 to 0.63, with increase in the concentration of the magnetic nanoparticles, respectively.

The effect of increasing the concentration of hybrid protein fibrils at constant protein/nanoparticles composition and under exposure of a fixed magnetic

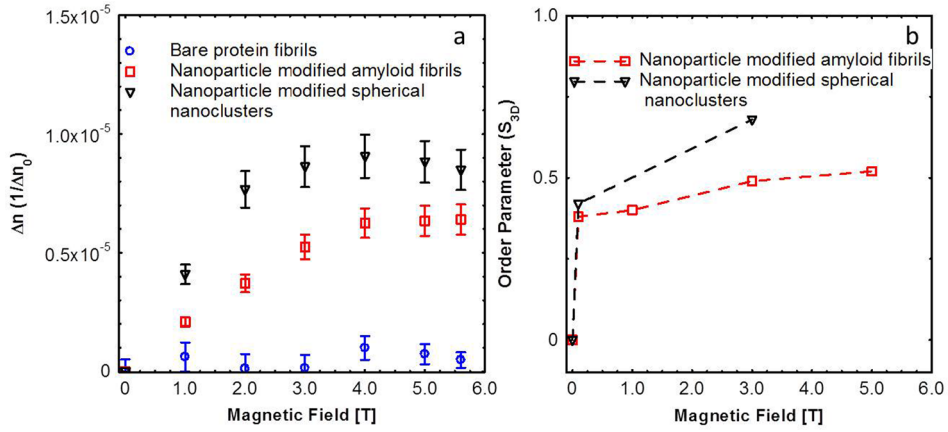

Figure 7. (a) Change of optical birefringence for bare protein fibrils (blue circles), nanoparticle-modified amyloid fibrils (0.3 wt % protein, 0.6 wt % nanoparticles, red squares) and nanoparticle-modified spherical nanoclusters (0.2 wt % protein, 0.6 wt % nanoparticle, - black triangles) at different magnetic field strengths. (b) Evolution of the order parameter S_{3D} of the aggregates in part (a) as a function of different magnetic field intensities.

field of 3 T was also briefly investigated by SANS. Initially, hybrid amyloid fibrils were prepared at the protein concentration of 2 wt % with 0.6 wt % nanoparticles, and the final amyloid fibrils concentrations were adjusted to 0.3, 1, and 5 wt % prior to the measurement. The 2D scattering patterns for concentrations of 0.3, 1, and 5 wt % hybrid fibrils are shown in the Supporting Information Figure S9 after applying an external magnetic field of 3 T. The scattering pattern at 1 wt % (Figure S9b) is clearly more anisotropic than what recorded at 0.3 wt % (Figure S9a): in this regime of concentration, where the nematic phase is expected also for pristine β-lactoglobulin fibrils,[42] both excluded volume interactions and the external magnetic field do contribute to the alignment of the fibrils, leading to an increased alignment with concentration. When the fibrils' concentration, however, reaches 5 wt %, the fibrils form a gel, in which physical interactions among contacting fibrils smear the overall alignment, leading to the isotropic 2D SANS pattern observed in Figure S9c, and as expected for isotropic physical gels.

Comparison of Alignment of Nanoparticle-Modified Amyloid Fibrils and Spherical Nanoclusters. Optical microscopy, AFM and SANS allow assessing the alignment of both amyloid fibrils and spherical nanoclusters at length scales intrinsically related to the resolution of the specific technique used. To quantify the spatial alignment of these hybrid aggregates induced by the presence of an external magnetic field, in bulk and at macroscopic (>wavelength of light) length scales, we also used the optical birefringence technique.[50] The change of the birefringence of bare protein fibrils, nanoparticle-modified amyloid fibrils and nanoparticle-modified spherical nanoclusters is shown in Figure 7a as a function of increasing magnetic field intensity. At zero magnetic field intensity, the birefringence is zero for all the samples. Furthermore, the bare amyloid fibrils show zero birefringence at all magnetic field strengths up to 5.5 T, as expected based on the low magnetic susceptibility of pure protein-based aggregates. However, when magnetic nanoparticles are embedded in the amyloid fibrils, birefringence starts to rise rapidly with increase in magnetic field intensity, confirming macroscopic alignment of the fibrils. The birefringence values of the nanoparticle-modified spherical nanoclusters prepared at pH 4.5 exhibit even higher values compared to the nanoparticle-modified amyloid fibrils, which infers a better alignment for the spherical nanoclusters. This is consistent with the values of the 3D order parameters for both classes of aggregates as a function of magnetic field, as determined by eq 1 on the corresponding SANS profiles and shown in Figure 7b. Thus, the various techniques used all confirm independently that both spherical and fibrillar hybrid aggregates can be efficiently aligned by an external magnetic field, with the spherical aggregates being slightly more efficient in achieving a cooperative alignment, possibly due to their improved mobility associated with the lower hydrodynamic radii.

Magnetic-Responsive Sol–Gel Transition. We finally explored the possibility of tuning the sol–gel transition in the nanoparticle-modified amyloid fibrils by using the external magnetic field. To this end, the ionic strength of a 2 wt % solution of nanoparticles-modified amyloid fibrils prepared at pH 3 was increased by adding 150 mM NaCl. Under these conditions, protein fibrils form a gel due to the screening of the electrostatic repulsive forces between the fibrils, leading hydrophobic and van der Waals attractive forces to dominate, and inducing physical cross-links among fibrils.[42] Figure 8a shows the nonflowing gel aspect of the hybrid fibrils prepared as discussed above. Interestingly, after the application of a magnetic field of intensity 1.1 T (using a Halbach magnet), the gel turns into a solution and starts flowing again, as shown in Figure 8b. This is a consequence of the fact that the

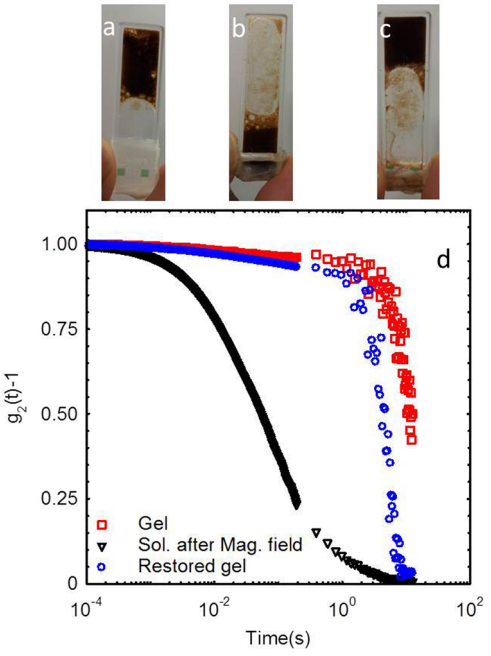

Figure 8. (a) Visual aspect of the gel-like behavior of nanoparticle-modified amyloid fibrils after addition of 150 mM NaCl salt. (b) Gel−sol transition during exposure to 1.1 T magnetic field and (c) recovery of the gel after removing the magnetic field. (d) Autocorrelation function of the electric field acquired by diffusive wave spectroscopy for nanoparticle-modified amyloid fibrils in presence of 150 mM NaCl. Red: prior to exposure to the magnetic field, indicating gel-like behavior. Black: during exposure to 1.1 T magnetic field, indicating solution-like behavior. Blue: restored gel after removing the magnetic field.

magnetic field induces alignment of fibrils into a strongly oriented nematic phase, which, due to the reduced excluded volume, minimizes the number of intermolecular contacts among fibrils, and thus suppresses the physical gel behavior. After removing the magnetic field, the solution reverts back to the pristine gel, due to the increased excluded volume interactions and interfibrillar physical contacts, as shown in Figure 8c.

To quantify this responsive gelation behavior independently, we used diffusive wave spectroscopy. The auto correlation functions of the electric field, $g_2(t) - 1$, before and after exposure to the magnetic field, are shown in Figure 8d. The auto correlation function before exposure to the magnetic field does not decay to zero, due to the nonergodic gel-like behavior. However after applying the magnetic field, the auto correlation function does relax to zero and shows a fast decay time, as expected for ergodic solution systems. As expected based on visual inspection (Figure 8b,c), the hybrid protein fibrils show self-healing behavior:[42] upon removal of the magnetic field, the physical interactions between fibrils are restored, ultimately causing again the formation of the gel. The autocorrelation function of the restored gel shows slow decay time (Figure 8d), inferring that the topology of the healed network is similar to that of the pristine gel and that the sol−gel behavior is entirely reversible.

CONCLUSIONS

Magnetic-responsive biohybrids of Fe_3O_4 nanoparticles and β-lactoglobulin, in the form of either fibrils or spherical nanoclusters, have been synthesized. The synthesis procedure involves first electrostatic complexation of proteins and nanoparticles, followed by a heating protocol, which induces the proteins to denature and aggregate into either amyloid fibrils or spherical nanoclusters, depending on temperature and pH used. In this self-assembly process, the protein plays the role of gluing together the magnetic nanoparticles and controls the final morphology of the hybrid aggregate. These hybrids can be aligned in three dimensions using magnetic fields of intensity as low as 0.1 T. Their alignment has been investigated by SANS, optical birefringence, optical microscopy and AFM. Analysis of the 2D and 3D order parameters, extracted from microscopy and scattering techniques, respectively, shows that the alignment of these structures is strongly dependent on both the intensity of the magnetic field and the concentration of the nanoparticles in the hybrids. Furthermore, the alignment is completely reversible on the ON/OFF state of the external magnetic field, and this, over several cycles of its application and removal. Finally, we have shown that the sol−gel transition in hybrid nanoparticle modified amyloid fibrils can be manipulated by using an external magnetic field, providing the possibility of converting, reversibly and iteratively, the protein gel into a liquid colloidal dispersion upon application/removal of the external magnetic field. This is a consequence of the reduced excluded volume of the amyloid fibrils in the aligned state (magnetic field ON), which decreases the average number of physical contacts among fibrils, converting the physical gel into a liquid. Due to the moderate intensity of the magnetic field used, its noninvasive nature, and the biocompatibility of the β-lactoglobulin-nanoparticle hybrid fibrils, this stimuli-responsive reversible sol−gel transition may find useful applications in several area of bionanotechnology.

MATERIALS AND METHODS

Biopure bovine β-lactoglobulin (lot JE 002-8-415) was kindly donated by Davisco Foods International (Le Seur, MN) and anionic magnetic iron nanoparticles (10 nm) were purchased from Ferrotec Corporation (anionic EMG-705). β-Lactoglobulin protein purification was performed following a procedure described by Jung *et al.*[51] In brief, β-lactoglobulin protein solutions were purified by centrifugal filtration followed by dialysis for 5 days. After purification, the protein solutions were adjusted to pH 2 and lyophilized.

The synthesis of hybrid iron nanoparticle modified amyloid fibrils and spherical nanoclusters used for the alignment study is prepared at various concentrations and discussed comprehensively in the results section. In brief, for the nanoparticle-modified spherical nanoclusters, protein monomers and iron nanoparticles are mixed at pH 4.5, followed by heating at 55 °C for 15 min. For the nanoparticle-modified amyloid fibril aggregates, protein monomers and iron nanoparticles are mixed at pH 3, followed by heating at 90 °C for 5 h.

Characterization Methods. Atomic force microscopy (AFM) in tapping mode was carried out on a Multimode 8 Scanning Force Microscope (Bruker). MPP-11100-10 tips for tapping mode in soft tapping conditions were used (Bruker) at a vibrating frequency of 300 kHz. The images were simply flattened using the Nanoscope 8.1 software.

Small angle neutron scattering (SANS) was used to investigate the structure[52] and the spatial alignment of nanostructures.[53,54] The facilities provided by SANS-II at PSI, Villigen, allow inducing the external magnetic force of different field strengths to the sample environment. The incident beam had a wavelength of λ = 0.5269 nm, and the sample to detector distance was varied between 1.2 and 6 m, corresponding to a q range of 0.05−2.4 nm^{-1}. The 2D scattering spectra were azimuthally averaged after correction of the background and the transmission. D_2O solvent was chosen instead of H_2O due to the better contrast for neutron scattering measurements. The scattered intensity *versus* azimuthal angle spectra were used to calculate the order parameter. Magnetic fields in the range of 0−5 T were applied using an electromagnet. The sample solutions were equilibrated for minimum 30 min at the magnetic field strength of interest before starting the measurements. Order parameters were extracted from azimuthal intensities measured in triplicate samples.

Polarized optical microscopy was performed using a Zeiss Axioskop 2 instrument. The magnetic field was applied by using a permanent magnet having field strength of 0.1 T.

Spatial alignment of protein aggregates ultimately develops the optical birefringence. Thus, a quick assessment of the protein aggregates alignment at various magnetic field strengths can be done by quantifying the resulting optical birefringence.[55,56] We measured the change in the optical birefringence of iron coated protein aggregates based on the phase modulation technique. A photoelastic modulator (PEM-90, Hinds Instruments), set to an operating frequency of 50 kHz, was placed between two crossed linear polarizers (Newport, Irvine, CA); a diode laser (Newport, Irvine, CA) with a wavelength (λ) of 635 nm was used as light source. The first and second harmonic, $I_1\omega$ and $I_2\omega$, of the AC signal were detected with two lock-in amplifiers (SR830, SRS, Sunnyvale, CA). The PEM amplitude A_0 was chosen to be 2.405 rad, therefore, making the DC component birefringence-independent. The birefringence Δn is obtained using:

$$\Delta n = \frac{\delta\lambda}{2\pi d} \qquad (2)$$

where d is the sample thickness and δ = arctan $\{[I_{1\omega}J_2(A_0)]/[I_{2\omega}J_1(A_0)]\}$, where J_1 and J_2 are the Bessel functions with $J_1(2.405) = 0.5191$ and $J_2(2.405) = 0.4317$.

Diffusive wave spectroscopy measurements were performed using a commercial DWS apparatus (LS instruments, Fribourg, Switzerland) having laser wavelength of 683 nm. The gel samples were directly prepared inside flat glass cells having optical path length of 2 cm, by mixing nanoparticles modified 2 wt % of amyloid fibrils (pH 3) with 150 mM NaCl. The intensity fluctuations were measured by a digital correlator and the electric field auto correlation function ($g_2(t) - 1$) was determined. Multispeckle spin echo method was used to calculate the long correlation time. The temperature of the sample was maintained at 25 °C by a Peltier temperature controller.

Light scattering experiments were performed using a 3D cross correlation spectrometer (LS instruments) equipped with a HeNe laser (λ = 632.8 nm). The time-averaged intensity correlation function was measured at a constant scattering angle ($\theta = 90°$) and the data were analyzed by CONTIN method.

Conflict of Interest: The authors declare no competing financial interest.

Acknowledgment. The authors acknowledge Dr. Urs Gasser (SANS II, PSI, Villigen) for assistance during the small angle neutron scattering experiments. Marianne Liebi (ETHZ), Stephan Handschin (ETHZ) and Dr. Randall Erb (ETHZ) are gratefully acknowledged for assistance during the birefringence and microscopy characterization experiments.

Supporting Information Available: Dynamic light scattering of the nanoparticles, additional TEM images, optical microscopy, AFM images, small angle neutron scattering data and a video of alignment of hybrid protein nanoclusters under exposure to a magnetic field. This material is available free of charge *via* the Internet at http://pubs.acs.org.

REFERENCES AND NOTES

1. Dickerson, M. B.; Sandhage, K. H.; Naik, R. R. Protein and Peptide Directed Syntheses of Inorganic Materials. *Chem. Rev.* **2008**, *108*, 4935–4978.
2. Olsson, R. T.; Samir, M. A. S. A.; Salazar-Alvarez, G.; Belova, L.; Ström, V.; Berglund, L. A.; Ikkala, O.; Nogués, J.; Gedde, U. W. Making Flexible Magnetic Aerogels and Stiff Magnetic Nanopaper using Cellulose Nanofibrils as Templates. *Nat. Nanotechnol.* **2010**, *5*, 584–588.
3. Hu, B.; Li, M.; Sadasivan, S.; Patil, A. J.; Mann, S. Fabrication of Functional Bioinorganic Nanoconstructs by Polymer−Silica Wrapping of Individual Myoglobin Molecules. *Nanoscale* **2011**, *3*, 1031–1036.
4. Zhang, T.; Wang, W.; Zhang, D.; Zhang, X.; Ma, Y.; Zhou, Y.; Qi, L. Biotemplated Synthesis of Gold Nanoparticle−Bacteria Cellulose Nanofiber Nanocomposites and Their Application in Biosensing. *Adv. Funct. Mater.* **2010**, *20*, 1152–1160.
5. Nicole, L.; Rozes, L.; Sanchez, C. Integrative Approaches to Hybrid Multifunctional Materials: From Multidisciplinary Research to Applied Technologies. *Adv. Mater.* **2010**, *22*, 3208–3214.
6. Ruiz-Hitzky, E.; Ariga, K.; Lvov, Y. M. *Bio-inorganic Hybrid Nanomaterials*; Wiley: Weinheim, Germany, 2008.
7. Lu, A. H.; Salabas, E. L.; Schueth, F. Magnetic Nanoparticles: Synthesis, Protection, Functionalization and Application. *Angew. Chem., Int. Ed.* **2007**, *46*, 1222–1244.
8. Mahmoudi, M.; Quinlan-Pluck, F.; Monopoli, M. P.; Sheibani, S.; Vali, H.; Dawson, K. A.; Lynch, I. Influence of the Physiochemical Properties of Superparamagnetic Iron Oxide Nanoparticles on Amyloid β Protein Fibrillation in Solution. *ACS Chem. Neurosci.* **2013**, *4*, 475–485.
9. Yoo, D.; Lee, J.-H.; Shin, T. H.; Cheon, J. Theranostic Magnetic Nanoparticles. *Acc. Chem. Res.* **2011**, *44*, 863–874.
10. Song, E. Q.; Hu, J.; Wen, C. Y.; Tian, Z. Q.; Yu, X.; Zhang, Z. L.; Shi, Y. B.; Pang, D. W. Fluorescent Magnetic Biotargeting Multifunctional Nanobioprobes for Detecting and Isolating Multiple Types of Tumor Cells. *ACS Nano* **2011**, *5*, 761–770.
11. Peterson, V. M.; Castro, C. M.; Lee, H.; Weissleder, R. Orthogonal Amplification of Nanoparticles for Improved Diagnostic Sensing. *ACS Nano* **2012**, *6*, 3506–3513.
12. Jun, Y. W.; Huh, Y. M.; Choi, J. S.; Lee, J. H.; Song, H. T.; Kim, S.; Yoon, S.; Kim, K. S.; Shin, J. S.; Suh, J. S.; *et al.* Nanosize Scale Effect of Magnetic Nanocrystals and Their Utilization for Cancer Diagnosis *via* Magnetic Resonance Imaging. *J. Am. Chem. Soc.* **2005**, *127*, 5732–5733.
13. Li, X.; Xu, H.; Chen, Z. S.; Chen, G. Biosynthesis of Nanoparticles by Microorganisms and Their Applications. *J. Nanomater.* **2011**, *2011*, 1–16.
14. Alphandéry, E.; Faure, S.; Seksek, O.; Guyot, F.; Chebbi, I. Chains of Magnetosomes Extracted from AMB-1 Magnetotactic Bacteria for Application in Alternative Magnetic Field Cancer Therapy. *ACS Nano* **2011**, *5*, 6279–6296.
15. Reiss, B. D.; Mao, C.; Solis, D. J.; Ryan, K. S.; Thomson, T.; Belcher, A. M. Biological Routes to Metal Alloy Ferromagnetic Nanostructures. *Nano Lett.* **2004**, *4*, 1127–1132.
16. Evans, B. A.; Shields, A. R.; Carroll, R. L.; Washburn, S.; Falvo, M. R. Superfine, R. Magnetically Actuated Nanorod Arrays as Biomimetic Cilia. *Nano Lett.* **2007**, *7*, 1428–1434.

17. Goubault, C.; Jop, P.; Fermigier, M.; Baudry, J.; Bertrand, E.; Bibette, J. Flexible Magnetic Filaments as Micromechanical Sensors. *Phys. Rev. Lett.* **2003**, *91*, 260802.
18. Kim, J.; Chung, S. E.; Choi, S. E.; Lee, H.; Kim, J.; Kwon, S. Programming Magnetic Anisotropy in Polymeric Microactuators. *Nat. Mater.* **2011**, *10*, 747–752.
19. Wang, X.; Song, J.; Liu, J.; Wang, Z. L. Direct-Current Nanogenerator Driven by Ultrasonic Waves. *Science* **2007**, *316*, 102–105.
20. Li, L. S.; Walda, J.; Manna, L.; Alivisatos, A. P. Semiconductor nanorod liquid crystals. *Nano Lett.* **2002**, *2*, 557–560.
21. Zhu, Y. F.; Ma, C.; Zhang, W.; Zhang, R. P.; Koratkar, N.; Liang, J. Alignment of Multiwalled Carbon Nanotubes in Bulk Epoxy Composites *via* Electric Field. *J. Appl. Phys.* **2009**, *105*, 054319.
22. Su, B.; Wu, Y.; Jiang, L. The Art of Aligning One-Dimensional (1D) Nanostructures. *Chem. Soc. Rev.* **2012**, *41*, 7832–7856.
23. Chew, S. Y.; Mi, R.; Hoke, A.; Leong, K. W. Aligned Protein–Polymer Composite Fibers Enhance Nerve Regeneration: A Potential Tissue-Engineering Platform. *Adv. Funct. Mater.* **2007**, *17*, 1288–1296.
24. Nie, Z.; Petukhova, A.; Kumacheva, E. Properties and Emerging Applications of Self-Assembled Structures Made from Inorganic Nanoparticles. *Nat. Nanotechnol.* **2010**, *5*, 15–25.
25. Reches, M.; Gazit, E. Controlled Patterning of Aligned Self-Assembled Peptide Nanotubes. *Nat. Nanotechnol.* **2006**, *1*, 195–200.
26. Caswell, K. K.; Wilson, J. N.; Bunz, U. H. F.; Murphy, C. J. Preferential End-to-End Assembly of Gold Nanorods by Biotin–Streptavidin Connectors. *J. Am. Chem. Soc.* **2003**, *125*, 13914–13915.
27. Huang, X.; Li, L.; Luo, X.; Zhu, X.; Li, G. Orientation-Controlled Synthesis and Ferromagnetism of Single Crystalline Co Nanowire Arrays. *J. Phys. Chem. C* **2008**, *112*, 1468–1472.
28. Tao, A.; Kim, F.; Hess, C.; Goldberger, J.; He, R.; Sun, Y.; Xia, Y.; Yang, P. Langmuir–Blodgett Silver Nanowire Monolayers for Molecular Sensing Using Surface-Enhanced Raman Spectroscopy. *Nano Lett.* **2003**, *3*, 1229–1233.
29. Gupta, S.; Zhang, Q.; Emrick, T.; Russell, T. P. Self-Corralling Nanorods under an Applied Electric Field. *Nano Lett.* **2006**, *6*, 2066–2069.
30. Hangarter, C. M.; Rheem, Y.; Yoo, B.; Yang, E. H.; Myung, N. V. Hierarchical Magnetic Assembly of Nanowires. *Nanotechnology* **2007**, *18*, 205305.
31. Skaat, H.; Sorci, M.; Belfort, G.; Margel, S. Effect of Maghemite Nanoparticles on Insulin Amyloid Fibril Formation: Selective Labeling, Kinetics, and Fibril Removal by a Magnetic Field. *J. Biomed. Mater. Res., Part A* **2009**, *91*, 342–351.
32. Hill, R. J. A.; Sedman, V. L.; Allen, S.; Williams, P.; Paoli, M.; Adler-Abramovich, L.; Gazit, E.; Eaves, L.; Tendler, S. J. B. Alignment of Aromatic Peptide Tubes in Strong Magnetic Fields. *Adv. Mater.* **2007**, *19*, 4474–4479.
33. Andersson, B. V.; Skoglund, C.; Uvdal, K.; Solin, N. Preparation of Amyloid-like Fibrils Containing Magnetic Iron Oxide Nanoparticles: Effect of Protein Aggregation on Proton Relaxivity. *Biochem. Biophys. Res. Commun.* **2012**, *419*, 682–686.
34. Korneva, G.; Ye, H.; Gogotsi, Y.; Halverson, D.; Friedman, G.; Bradley, J. C.; Kornev, K. G. Carbon Nanotubes Loaded with Magnetic Particles. *Nano Lett.* **2005**, *5*, 879–884.
35. Skaat, H.; Shafir, G.; Margel, S. Acceleration and Inhibition of Amyloid Fibril Formation by Peptide-Conjugated Fluorescent Maghemite Nanoparticles. *J. Nanopart. Res.* **2011**, *13*, 3521–3534.
36. Xu, Y.; Yuan, J.; Fang, B.; Drechsler, M.; Müllner, M.; Bolisetty, S.; Ballauff, M.; Müller, A. H. E. Hybrids of Magnetic Nanoparticles with Double-Hydrophilic Core/Shell Cylindrical Polymer Brushes and Their Alignment in a Magnetic Field. *Adv. Funct. Mater.* **2010**, *20*, 4182–4189.
37. Bolisetty, S.; Vallooran, J. J.; Adamcik, J.; Handschin, S.; Gramm, F.; Mezzenga, R. Amyloid-Mediated Synthesis of Giant, Fluorescent, Gold Single Crystals and Their Hybrid Sandwiched Composites Driven by Liquid Crystalline Interactions. *J. Colloid Interface Sci.* **2011**, *361*, 90–96.
38. Bolisetty, S.; Adamcik, J.; Heier, J.; Mezzenga, R. Amyloid Directed Synthesis of Titanium Dioxide Nanowires and Their Applications in Hybrid Photovoltaic Devices. *Adv. Funct. Mater.* **2012**, *22*, 3424–3428.
39. Amar-Yuli, I.; Adamcik, J.; Lara, C.; Bolisetty, S.; Vallooran, J. J.; Mezzenga, R. Templating Effects of Lyotropic Liquid Crystals in the Encapsulation of Amyloid Fibrils and Their Stimuli-Responsive Magnetic Behavior. *Soft Matter* **2011**, *7*, 3348–3357.
40. Ahn, S.; Kasi, R. M.; Kim, S. C.; Sharma, N.; Zhou, Y. Stimuli-Responsive Polymer Gels. *Soft Matter* **2008**, *4*, 1151–1157.
41. Mitsumata, T.; Furukawa, K.; Juliac, E.; Iwakura, K.; Koyama, K. Compressive Modulus Of Ferrite Containing Polymer Gels. *Int. J. Mod. Phys. B* **2002**, *16*, 2419–2425.
42. Bolisetty, S.; Harnau, L.; Jung, J. M.; Mezzenga, R. Gelation, Phase Behavior, and Dynamics of β-Lactoglobulin Amyloid Fibrils at Varying Concentrations and Ionic Strengths. *Biomacromolecules* **2012**, *13*, 3241–3252.
43. Lu, Z.; Yin, Y. Colloidal Nanoparticle Clusters: Functional Materials by Design. *Chem. Soc. Rev.* **2012**, *41*, 6874–6887.
44. Li, F.; Chen, H.; Zhang, Y.; Chen, Z.; Zhang, Z. P.; Zhang, X. E.; Wang, Q. Three-Dimensional Gold Nanoparticle Clusters with Tunable Cores Templated by a Viral Protein Scaffold. *Small* **2012**, *8*, 3832–3838.
45. Paquet, C.; Pagé, L.; Kell, A.; Simard, B. Nanobeads Highly Loaded with Superparamagnetic Nanoparticles Prepared by Emulsification and Seeded-Emulsion Polymerization. *Langmuir* **2010**, *26*, 5388–5396.
46. Sears, V. F. Neutron Scattering Lengths and Cross Sections. *Neutron News* **1992**, *3*, 26–37.
47. Mitchell, G. R.; Windle, A. H. In *Developments in Crystalline Polymers*; Bassett, D. C., Ed; Elsevier: London,1988; Vol. 2.
48. Mezzenga, R.; Jung, J. M.; Adamcik, J. Effects of Charge Double Layer and Colloidal Aggregation on the Isotropic–Nematic Transition of Protein Fibers in Water. *Langmuir* **2010**, *26*, 10401–10405.
49. Adamcik, J.; Jung, J. M.; Flakowski, J.; Rios, P. D. L.; Dietler, G.; Mezzenga, R. Understanding Amyloid Aggregation by Statistical Analysis of Atomic Force Microscopy Images. *Nat. Nanotechnol.* **2010**, *5*, 423–428.
50. Liebi, M.; Kohlbrecher, J.; Ishikawa, T.; Fischer, P.; Walde, P.; Windhab, E. J. Cholesterol Increases the Magnetic Aligning of Bicellar Disks from an Aqueous Mixture of DMPC and DMPE–DTPA with Complexed Thulium Ions. *Langmuir* **2012**, *28*, 10905–10915.
51. Jung, J. M.; Savin, G.; Pouzot, M.; Schmitt, C.; Mezzenga, R. Structure of Heat-Induced Beta-Lactoglobulin Aggregates and Their Complexes with Sodium-Dodecyl Sulfate. *Biomacromolecules* **2008**, *9*, 2477–2486.
52. Pedersen, J. S. Analysis of Small-Angle Scattering Data from Colloids and Polymer Solutions: Modeling and Least-Squares Fitting. *Adv. Colloid Interface Sci.* **1997**, *70*, 171–210.
53. Wang, H.; Xu, Z.; Eres, G. Order in Vertically Aligned Carbon Nanotube Arrays. *Appl. Phys. Lett.* **2006**, *88*, 213111–3.
54. Lee, J. H.; Choi, S. M.; Pate, B. D.; Chisholm, M. H.; Han, Y. S. Magnetic Uniaxial Alignment of the Columnar Superstructure of Discotic Metallomesogens over the Centimetre Length Scale. *J. Mater. Chem.* **2006**, *16*, 2785–2791.
55. Torbet, J.; Ronziere, M. C. Magnetic Alignment of Collagen during Self-Assembly. *Biochem. J.* **1984**, *219*, 1057–1059.
56. Lewis, B. A.; Rosenblatt, C.; Griffin, R. G.; Courtemanche, J.; Herzfeld, J. Magnetic Birefringence Studies of Dilute Purple Membrane Suspensions. *Biophys. J.* **1985**, *47*, 143–150.